

# Design and characterisation of multi-cavity, fluidic haptic feedback system for mechano-tactile feedback

Ge Shi, Jialei Shi, Azadeh Shariati, Kamyar Motaghedolhagh, Shervanthi Homer-Vanniasinkam  
Helge Wurdemann

**Abstract**—Numerous studies have indicated that the use of a closed-loop haptic feedback system, which offers various mechano-tactile stimuli patterns with different actuation methods, can improve the performance and grasp control of prosthetic hands. Purely mechanical-driven feedback approaches for various mechano-tactile stimuli patterns, however, have not been explored. In this paper, a multi-cavity fluidic haptic feedback system is introduced with details of design, fabrication, and validation. The multi-cavity haptic feedback system can detect the physical touch with direction at the fingertip sensor. The direction of the force is reflected in the form of pressure deviation in the multi-cavity fingertip sensor. The feedback actuator generates various mechano-tactile stimuli patterns according to the pressure deviation from the fingertip sensor. Hence, users can identify the force with direction according to the stimuli patterns. The haptic feedback system is validated through two experiments. The initial experiment characterises the system and establishes the relationship between the fingertip sensor and feedback actuator. The subsequent experiment, a human interaction test, confirms the system's capability to detect force with directions and generate corresponding tactile stimuli in the feedback actuator. The outcomes corroborate the idea that participants are generally capable of discerning changes in angle.

**Index Terms**—Haptic Feedback System, Mechanotactile Stimulation, Soft Robotics, Upper-limb Prosthetics.

## I. INTRODUCTION

**A**MPUTATION of upper limbs causes a significant effect on the ability and functions in daily activities. According to data from the World Health Organization (WHO), 95% of the 40 million amputees in developing countries lack affordable prosthetic care [1]. Various reasons can lead to limb amputation, such as diabetes, traffic accidents, occupational injuries, polio, meningitis, and stroke [2]. Trauma has caused the majority of upper-limb amputations (31.5%) [3]. In particular, partial-hand amputations related to occupational injuries are the most frequently amputated body parts [2]. Regarding the severity, amputees may require long-term, frequent support to work and adapt to daily life. Hence,

G. Shi, J. Shi, A. Shariati, K. Motaghedolhagh, S.H. Vanniasinkam, H.A. Wurdemann are with the Department of Mechanical Engineering, University College London, London, United Kingdom. E-mail: h.wurdemann@ucl.ac.uk.

Ge Shi is also with the Robotics and Autonomous Systems, Data61, Commonwealth Scientific and Industrial Research Organisation, Brisbane, Australia.

Jialei Shi is also with the Mechatronics in Medicine, The Hamlyn Centre for Robotic Surgery, Department of Mechanical Engineering, Imperial College London, United Kingdom.

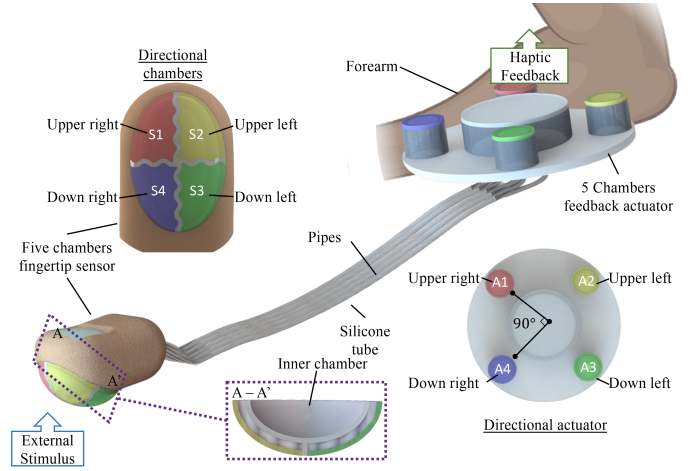


**Fig. 1.** CAD drawing of the five-chamber haptic feedback system. Five chambers in the fingertip sensor and feedback actuator are individually connected with silicone tubes. The four coloured cavities (red, yellow, green, and blue) with the labels S1, S2, S3, and S4 on the outer layer of the fingertip sensor are connected to the peripheral chambers in the feedback actuator with the same colour and numbers A1, A2, A3, and A4, respectively. The inner cavity is connected to the central chamber in the feedback actuator. The entire system is filled with water.

types of prosthetics are designed to help amputees, including cosmetics, body- and battery-powered devices [4]. Notable advancements in developing types of prostheses have been achieved to reproduce hand functionality. Cosmetic prosthetics are primarily designed for appearance rather than function, helping amputees achieve a natural look [5]. Body-powered prosthetics are mechanically operated by the wearer's own body movements. The system employs a series of cables, harnesses, and levers—much like a bicycle's brake system. The user's actions, such as chest expansion or waist bending, are translated into prosthetic limb movements, such as opening or closing a hand. These prosthetics, despite having some functional limitations, are appreciated for their reliability, cost-effectiveness, and suitability in low-resource settings [6], [7]. On the other hand, battery-powered or electric prosthetics use battery-driven motors for movement. These smart devices pick up Electromyography (EMG) signals from the remaining muscles in the amputee's limb to move the prosthetic. While they offer more control and precision, they are more complex and costly compared to body-powered prosthetics [5], [8], [9].

However, restoring the versatility of a hand is challenging, especially in terms of conveying sensory information.

Tactile sensation is crucial for adept manipulation of the human hand, and significant challenges emerge when such sensations are diminished or completely absent. There have been substantial advancements in equipping amputees with sensory perception using both invasive and non-invasive haptic feedback systems. A spectrum of systems, including static mechano-, vibro-, electro-tactile, and hybrid models, have been assessed in [10]–[12]. A range of mechano-tactile stimuli have been facilitated by the rigid mechanisms of the haptic feedback system, through skin stretch and indentation [13]–[16]. In [17], they provide a platform to deliver different kinds of tactile stimuli. There is an emerging trend towards haptic feedback systems with soft structures, owing to their user-friendly features and simple structure [18]–[20]. In [21], [22], soft elastic pockets were incorporated into the prosthetic socket to denote contact force by inflating the socket with a pump. Nevertheless, cost remains a significant factor for amputees. A pneumatically actuated soft sleeve was developed to provide users with a variety of tactile stimuli [23]. Moreover, the work by [24] offers a reconfigurable platform featuring various soft elastic structures for forearm tactile stimulation. Notably, purely mechanical-driven feedback methods associated with low costs have been relatively under-explored. The initial concept was introduced by Rosset [25] in 1933. Subsequently, Conzelman et al. were granted a patent in 1953 for the closed-loop sensory attachment which facilitates contact transmission in prosthetics. Initial studies concerning a pneumatic closed-loop haptic feedback system were undertaken and validated with subjects in [26]. A fluidic closed-loop haptic feedback system employing incompressible fluids has been validated with an analytical model [27], [28]. Existing research on fluidic haptic feedback systems has focused on single chamber designs to indicate physical contact. However, a multi-chamber system that can indicate both contact and direction is still undeveloped. Numerous studies suggest that employing a closed-loop haptic feedback system with multiple mechano-tactile stimuli patterns enhances the functionality and grasp control of prosthetic hands [29]–[32]. A haptic feedback system with multi-actuator generates vibro-tactile haptic patterns helping amputees to identify the contact location of the fingertips in a prosthetic hand [33]. However, a fluidic haptic feedback system has not been developed with a multi-actuation design to identify contact locations.

This paper introduces the design, fabrication, and characterisation of a multi-cavity, fluidic haptic feedback system featuring a soft-structure fingertip sensor and feedback actuator, illustrated in Fig. 1. The proposed haptic feedback system operates by converting tactile information captured by the fingertip sensor into mechanical pressure changes, which are then transmitted through fluid-filled channels to actuate soft actuators against the skin on the forearm, providing intuitive tactile feedback to the user. The contributions are:

- The development of a novel mechanically-driven, multi-cavity haptic feedback system designed to sense and indicate touch, including direction. The system adopts

an optimised soft structure within a coupled hydraulic system to generate varying tactile patterns.

- The proposed system is both lightweight and cost-effective due to its entirely mechanical nature, thereby eliminating the need for electronic components such as batteries or a micro-controller.

In applications for upper-limb prostheses, our haptic feedback system might enrich the user's sensory experience and control. As each fingertip provides an array of tactile forces, the system might allow amputees to precisely understand the direction and nature when in interaction with objects. This perception might enable users to perform complex tasks with greater accuracy, such as distinguishing between different textures or grasping objects of varying shapes and sizes.

Section II introduces the operating principles of the entire haptic interface, providing detailed descriptions of both the fingertip sensor and the feedback actuator. In Section III, the fabrication processes for the soft structures used in the fingertip sensor and feedback actuator are elucidated. An engineering characterisation of the proposed system, along with validation tests conducted with healthy subjects, are presented in Section IV, followed by a critical discussion in Section V. Section VI consolidates the key findings of this research and offers recommendations for future work.

## II. DESIGN OF THE HAPTIC FEEDBACK SYSTEM

The multi-chamber fluidic haptic feedback system presented in Fig. 1 shares features with the initial prototype described in [27], including being mechanically driven and capable of sensing physical interactions with objects, then subsequently transferring the tactile sensation back to the user. In order to sense and feedback not only the force level but also its direction, the haptic feedback system is designed with multi-cavity structure. It comprises two key components: a fingertip sensor and feedback actuators, each containing five cavities. A double-layered elastic membrane forms an ellipsoid shape at the fingertip, with four individual cavities in the outer layer and one in the inner layer. The four outer layer cavities follow a four-quadrant pattern. The feedback actuator also has five chambers with round-shaped membranes, with one central chamber and four peripheral chambers arranged circularly around the centre at 90° angles to each other.

In Fig. 1, the four outer layer chambers of the fingertip sensor, coloured red, yellow, green, and blue, are connected to the corresponding coloured peripheral chambers of the feedback actuator. The inner cavity connects to the central chamber of the feedback actuator. The mapping strategy ensures that force patterns on the forearm, mirroring those on the fingertip sensor, intuitively indicate the same direction of force at the prosthetic end. Altogether, the five fingertip sensor chambers connect to the feedback actuator chambers individually through silicone tubes, forming five independent closed-loop cavities filled with incompressible fluid water.

As the fingertip sensor interacts with objects from various angles, the five cavities deform responsively. Depending on the contact angles and object shapes, the five chambers exhibit different deformation patterns due to varying hydrostatic

pressure amplitudes. Given water's incompressible nature, the fluid flows to the feedback actuator as the chambers deform, pressurising the feedback actuator membranes individually and generating the tactile pattern detected by the fingertip sensor.

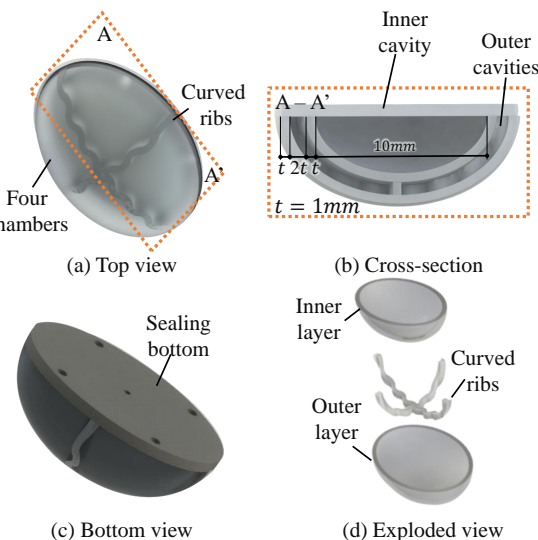
### A. Design of the fingertip sensor

Fig. 2(a) provides a general configuration of the fingertip sensor, which is ellipsoid shape with four quadrant chambers. Fig. 2(d) illustrates an exploded view of the fingertip sensor structure, which includes an outer layer, curved ribs, and an inner layer. In Fig. 2(b), the cross-section view of the fingertip sensor shows that both the inner and outer layers are 1 mm thick, while the curved ribs possess a height of 2 mm. In the fingertip sensor, the cavities in four quadrant chambers is  $144.02 \text{ mm}^3$ , and in inner cavity is  $314.16 \text{ mm}^3$ . The diameter of the inner cavity is 10 mm. The sensor comprises a total of five cavities—four arranged in a quadrant pattern within the outer layer and one formed within the inner layer. The curved design of the ribs reduces compression strength, thereby increase the flexibility during deformation, as the primary function of the ribs is to partition the cavities.

When the inner cavity deforms due to an intensive deformation, a considerable volume of liquid flows toward the enhance chamber in the feedback actuator. When the inner cavity is significantly deformed, a substantial volume of liquid is directed towards the enhancement chamber within the feedback actuator. Hence, the inner layer of the fingertip sensor acts as a sensor of a high force level touch on a prosthetic hand. In Fig. 2(c), the bottom of the double-layered membrane seals the five cavities, with round housing in corresponding positions to connect with pipes for water flow.

### B. Design of the feedback actuator

The aim of the feedback actuator is to react to pressure elevations in each cavity, creating tactile stimuli for users.



**Fig. 2.** The configuration of the double-layer fingertip sensor. (a) Top view (b) Cross-section view (c) Bottom view (d) Exploded view.

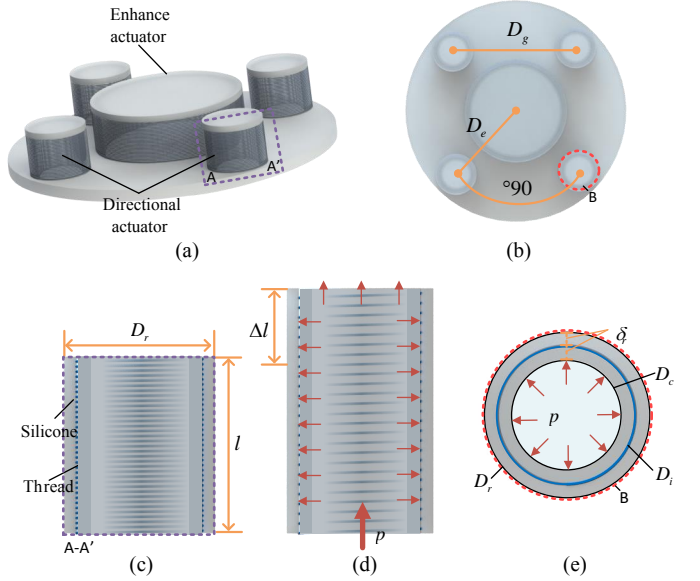


**Fig. 3.** Configuration of the feedback actuator:(a) General view of the feedback actuator. (b) Top view of the feedback actuator. (c) Side-section view of a linear actuator. (d) Side-section view of an actuated actuator by a pressure  $p$ . (e) Cross-section view of a linear actuator

Though membrane inflation has proven effective in generating mechano-tactile stimuli as shown in [21], [22], the limited volume of the cavities in the fingertip sensor necessitates a design to minimise inefficient deformation for tactile stimuli. Thus, an optimised linear actuator, characterised by a thread-reinforced cylindrical geometry, is utilised, which exhibits elongation when subjected to pressure.

Thread reinforcement, first introduced in [34], has been widely utilised to control motion of soft actuators in various applications [35]–[40]. Studies comparing thread-reinforced soft actuators have shown that reinforcement significantly reduces the ballooning effect, allowing for up to ten times higher deformation with hydraulic actuation in desired areas [41], [42]. Thread reinforcement minimises lateral inflation and increases actuation efficiency to achieve intended motions, as compared to flat membrane inflation. Upon pressure application to the actuator chamber, the thread enhances the radial stiffness of the cylindrical chambers, causing them to elongate rather than inflating in all directions.

The five cavities of the fingertip sensor are connected to five linear actuators to generate tactile patterns. Fig. 3(b) displays how four directional actuators surround the central intensifier actuator. According to [43], the minimum distance

TABLE I: Design specification of feedback actuators

Symbol	Definition	Value & Unit(mm)
$l$	Length of actuators	D&C:15
$D_r$	Outer diameter of actuators	D:10&C:35
$D_c$	Inner diameter of actuators	D:8.5&C:33.5
$D_i$	Diameter of threads	D:9.25&C:34.25
$D_g$	Distance of two directional actuators	D:40
$D_e$	Distance of directional to the enhance	D:20
$\delta_r$	Thickness of silicone layers	D&C:0.75

\* Design parameters with D: Directional chambers, C: Central chamber.

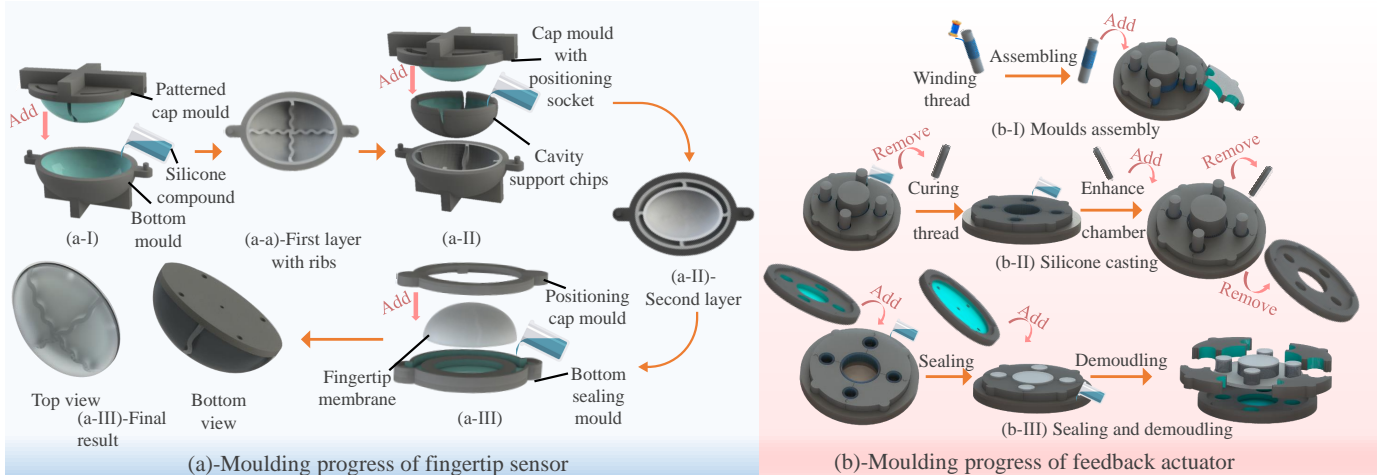


**Fig. 4.** In the fabrication process of the haptic feedback system, moulds highlighted with blue colour means the surface is in contact with silicone compound. (a) Moulding progress of the fingertip sensor: (b) Diagram of fabrication of the feedback actuator

necessary for two-point touch discrimination on the forearm is 40 mm. This value offers critical insights into the spatial resolution of tactile sensations on the forearm. Therefore, the gap from the centroid of each side directional actuator,  $D_g$ , is 40 mm. Consequently, users can distinguish each point of stimuli from directional chambers when both chambers engage simultaneously. The  $D_e$ , representing the centroid distance between the intensify actuator and the directional actuator, is 20 mm. As a result, the user perceives only one point of stimuli while the directional and intensify actuators are activated simultaneously. When the intensive deformation happened at the fingertip sensor, user will feel the extensive tactile stimuli when the enhance actuator is actuated. Thus, the contribution of the enhanced chamber is to serve as an indicator, signalling when the prosthetic hand is engaging in a grasp that involves a high force level. This feature provides users with intuitive feedback about the intensity of their grip. In Fig. 3(e), a cross-sectional view of the linear actuator shows the elastic silicone (grey) and embedded thread (blue circle). The outer diameter  $D_r$  is 10 mm, the inner diameter  $D_c$  is 8.5 mm, and the embedded thread has a diameter of 9.25 mm. Table I summarises the design specifications. In the feedback actuator, the cavities in four directional chambers is  $56.74 \text{ mm}^3$ , and in inner cavity is  $880.97 \text{ mm}^3$

### III. FABRICATION OF THE HAPTIC FEEDBACK SYSTEM

To create a durable, purely mechanically driven haptic feedback system filled with water, silicone polymer was chosen for fabricating the fingertip sensor and feedback actuator due to its softness, skin-friendly, robustness, and waterproof properties. The Dragon Skin 20 series was selected to create the fingertip sensor for its high elasticity, shape retention, and minimised pressure increase interaction in cavities. Ecoflex 0010 was chosen to cast the stretchable wall of each linear actuator, and the sealing layer of actuators utilises Dragonskin 30, a stiffer silicone. The soft feature of Ecoflex 0010 allows the linear actuator to elongate under pressure, generating more intense tactile stimuli. This difference in stiffness enhances the efficiency of pressurisation in producing tactile stimuli.

The manufacturing process of the fingertip sensor and feedback actuator is demonstrated in Fig. 4. Both devices employ moulding methods to fabricate. The surfaces of moulds coloured in blue represent the contact surface of the uncured silicone liquid and the shape of the cured silicone solid. The mixed silicone compound is prepared and degassed in a vacuum chamber using a vacuum pump at a vacuum pressure of  $-0.9$  bar, ready for pouring. The uncured silicone compound (viscous liquid) is poured into the mould and solidifies into an elastic material with the desired shape after curing. Casting moulds were designed using Solidworks (Dassault Systemes SE) and 3D printed by a Form 3+ printer (Formlabs Inc.) with photopolymer resin (Tough 2000 V1).

In order to maintain the consistency of the elastic components, the uncured compound has a mix weight ratio of 1:1, measured by a highly accurate weight scale (ACCT) with 0.01 g accuracy. During fabrication, this weight ratio was strictly maintained to ensure material consistency. Regarding the structure of soft components, including the fingertip sensor and feedback actuator, they were crafted using 3D-printed moulds from a Formlab 3B printer, which offers high accuracy with a 0.025 mm resolution. This printer ensures dimensional consistency for the moulds. Although the fabrication process involves manual operations, which could lead to inconsistencies at minor level, overall consistency remains high due to these stringent measures.

#### A. Fingertip sensor

The fabrication process of the fingertip sensor is illustrated in detail in Fig. 4(a). The double-layer soft structure of the fingertip sensor requires a three-step fabrication process for the outer and inner layer as well as for the bottom sealing, as outlined below.

*a) Outer layer:* The outer layer, inclusive of the ribs, is created using a two-part moulding technique. An ellipsoid-shaped mould base is loaded with uncured silicone, after which a corresponding positive mould is applied, ensuring precision. Upon curing of the silicone, excess material is meticulously

trimmed, ultimately yielding the outer layer adorned with curved ribs.

*b) Inner layer:* The creation of the inner layer commences while the outer layer with ribs is still retained within the mould base. Curved-edge support chips are introduced to preserve the volume of the outer layer's cavities throughout the casting process. These chips, in conjunction with the rib surfaces, establish an ellipsoid shape destined to form the inner layer. Uncured silicone is then dispensed into this setup and subsequently capped. The silicone adheres to the exposed rib surfaces upon curing. Following this, both the support chips and any surplus silicone are extracted, culminating in a double-layered ellipsoid membrane.

*c) Bottom sealing:* A two-part mould is utilised to seal the fingertip sensor using silicone. To prevent excess silicone from interfering with the design, a release spray (HD-SIL RELEASE, Ambersil) is coated to the exterior surface of the fingertip membrane. Uncured silicone is then poured into the lower section of the sealing mould, followed by the insertion of the double-layered fingertip sensor. A cap, equipped with a positioning hollow, is employed to guarantee a precise seal in accordance with the intended shape and size. Once the fingertip is sealed, silicone pipes are attached to the housing in the bottom layer using silicone glue (Sil-poxy, Smooth-on) for fluid flow.

### B. Haptic feedback actuator

The thread reinforced actuator requires three steps fabrication process, as outlined in Fig. 4(b). The thread (cotton) with a rough surface generates robust adhesion with the silicone solid, ensuring the thread experiences the same displacement as the attached silicone under pressurisation.

*a) Mould assembly:* Cotton thread is wrapped around the chamber moulds designated for each linear actuator. Four mould pieces are then assembled, generating five cylindrical chambers at the centre. A positioning plate, furnished with grooves and holes, is employed to secure the moulds together, thus guaranteeing the accuracy of the dimensions for the silicone after curing.

*b) Silicone casting:* Uncured silicone (Ecoflex 0010) is poured into the assembled moulds to create the actuator. Once cured, the chamber moulds are removed, leaving the thread embedded in the silicone. Smaller diameter chamber moulds are inserted and filled with silicone. After curing, the moulds are removed, forming a reinforced layer in each actuator to enhance durability and robustness.

*c) Sealing and demoulding:* A stiffer silicone (Dragon-skin 30A) is used to seal the actuators on both sides. By replacing the positioning plate with a mould, a stiffer layer is cured on the actuator's top. Silicone pipes are attached to the actuator's bottom using silicone glue (Sil-poxy, Smooth-on) for fluid flow. Finally, the mould components are removed, yielding the finished feedback actuator.

### C. System Assembly

The assembly of the haptic feedback system involves steps to ensure proper function and reliability. First, a syringe is

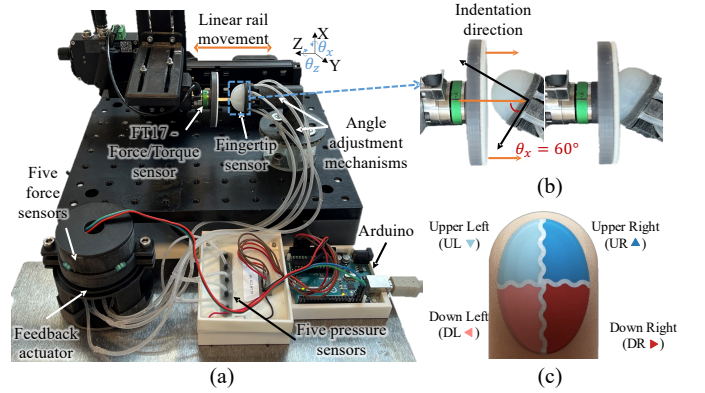


**Fig. 5.** The workbench of the characterising test for the five-chambers haptic feedback system: (a) The overview of the workbench setup. (b) Enlarged view of the fingertip sensor with compression angle at  $\theta_x = 0^\circ$ ,  $\theta_z = 60^\circ$  in the initial and the compressed state. (c) The schematic diagram of the outer layer of the fingertip sensor with the corresponding name.

used to fill the system with liquid. The components, including the fingertip sensor and feedback actuator, are then placed in water and put into a vacuum chamber to remove any air bubbles. This step is crucial to eliminate air pockets that could affect system performance.

After removing the air bubbles, the system is assembled underwater to keep the liquid intact and prevent air from entering. The components are then sealed with the silicone pipes and silicone glue to ensure a watertight seal, enhancing the system's durability. The hose connecting the fingertip sensor to the feedback actuator is 235 mm long. The inner diameter of the silicone tubes is 0.75 mm, and the outer diameter is 1.25 mm. These dimensions are essential for maintaining the system's fluid pathways and ensuring accurate haptic feedback.

## IV. VERIFICATION AND VALIDATION OF THE MECHANICAL-BASED HAPTIC FEEDBACK SYSTEM

Two experiments were carried out to evaluate and analyse the haptic feedback system. Firstly, the haptic feedback system was characterised with a workbench. The relationship of pressure, indentation, angle, and force between the fingertip sensor and the feedback actuator was determined. Section IV-B presents the human interaction test to identify the touching threshold, the direction of the force, and the level of the force.

### A. Experiment 1: Characterising the haptic feedback system

*Protocol:* This experiment was structured to characterise the physical correlation between the chambers in the fingertip sensor and the associated actuators in the feedback actuator using a single system. The force  $F_c$  applied to the fingertip sensor, the force  $F_f$  elicited by the feedback actuator, and the internal liquid pressure  $P_c$  of each closed-loop cavity in the haptic system were recorded. The fingertip sensor was indented by 4 mm at a rate of 5.81 mm/s at a variety of directions composed of rotation angle ( $\theta_x$ ) and pitch angle ( $\theta_z$ ). The choice of an indentation depth of 4 mm and a speed of 5.81 mm/s is based on research into human hand

grasping data from [44] and [45]. The selection is aimed to validating the system's relevance in real-world scenarios. Related data in the experiment, including angles ( $\theta_x$ ,  $\theta_z$ ), pressure, indentation, response force on the fingertip sensor, and the blocked force at the feedback actuator, was recorded via hardware sensors. Each scenario with different angles was tested five times, and an average was obtained from the trials.

To assess the capability of the sensor in discerning different contact angles via pressure differences among the five chambers, the experiment was conducted using a combination of angles. The rotation angle ( $\theta_x$ ) ranged from  $0^\circ$  to  $45^\circ$  with an interval of  $22.5^\circ$ , while the pitch angle ( $\theta_z$ ) varied between  $90^\circ$  and  $60^\circ$ , with a  $10^\circ$  increment. When  $\theta_z$  is  $90^\circ$ , the fingertip sensor is perpendicular to the force sensor. This alignment results in an equivalent level of indentation in each chamber of the fingertip sensor, regardless of the value of  $\theta_x$ . Hence, when  $\theta_z$  is set to  $90^\circ$ , only  $\theta_x$  at  $0^\circ$  was subjected to testing.

The pitch angle ( $\theta_z$ ) starts from  $60^\circ$ . If the value of  $\theta_z$  is less than  $60^\circ$ , the Force/Torque (F/T) sensor cannot provide the sufficient indentation of 3 mm to the fingertip sensor. The rotation angle ( $\theta_x$ ) range was determined based on the axis-symmetry of the sensor about its major and minor axes, given its ellipsoid shape. Therefore, the results within a range of  $0^\circ$  to  $90^\circ$  can be extrapolated to cover any indentation angle,  $\theta_x$ .

**Experimental setup:** The experimental workbench was constructed as shown in Fig. 5(a), including a linear rail (Zaber X LSM100A) with  $0.05 \mu\text{m}$  sensitivity, a 6-axis force/torque sen-

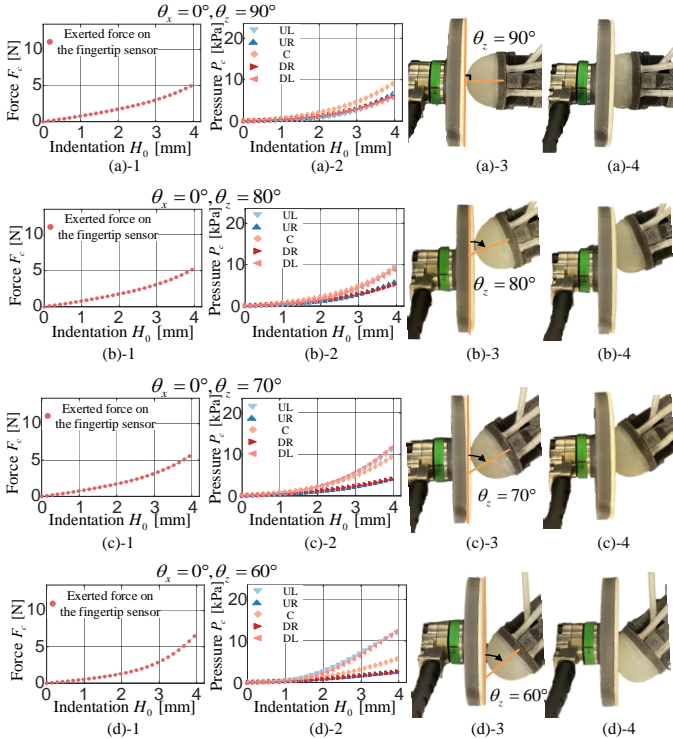


**Fig. 6.** Test data of compression with different pitch angles  $\theta_z$ . The first column shows the relationship between the fingertip force  $F_c$  and indentation  $H_0$ . The corresponding pressures  $P_c$  in five-cavities against the indentation  $H_0$  in the second column. The third and fourth columns present the enlarged view of the fingertip sensor with compression angles.

sor (IIT FT17) with  $0.318 \text{ mN}$  sensitivity, five membrane force sensors (MF01A-N-221, Alpha TW) with  $1.89 \text{ mN}$  sensitivity, and five pressure gauge sensors (ABPDANV015PGAA5, Honeywell) with  $0.033 \text{ kPa}$  sensitivity. The linear rail records the indentation applied to the fingertip sensor, while a 6-axis force/torque sensor measures the force exerted on the sensor. Pressure gauge sensors are utilised to monitor pressure changes within the five closed-loop cavities, and five membrane force sensors track the output force of the linear actuators within the feedback actuator system. A 3D-printed rigid mechanism is employed to adjust the rotation angle ( $\theta_x$ ) and pitch angle ( $\theta_z$ ) of the fingertip sensor. As depicted in Fig. 5(c), the outer layer chambers in the fingertip sensor are labelled as follows: Upper Left (UL) in light blue, Upper Right (UR) in dark blue, Down Left (DL) in light red, and Down Right (DR) in dark red.

**Test Results:** The test results related to indentation  $H_0$ , force exerted on the fingertip sensor  $F_c$ , and liquid pressure in the five closed-loop cavities  $P_c$  are shown in Figs. 6 and 7. The relationships between pressure  $P_c$  and blocked force  $F_f$  for the five actuators are represented in Fig. 8. The data associated with each cavity of the five cavities are colour-coded: light blue for upper left (UL), dark blue for upper right (UR), light red for down left (DL), dark red for down right (DR), and yellow for the center chamber (C). Overall, both the force on the fingertip sensor  $F_c$  and the pressures  $P_c$  display a non-linear increase relative to the indentation  $H_0$ , with pressures growing exponentially after  $H_0$  exceeds  $1.6 \text{ mm}$ . However, the variation in pressure across different chambers and force  $F_c$  on the fingertip sensor fluctuates in magnitude as the rotation angle  $\theta_x$  and the pitch angle  $\theta_z$  change.

In Fig. 6, the pitch angle  $\theta_z$  is varied from  $90^\circ$  to  $60^\circ$  in decrements of  $10^\circ$ . As shown in Fig. 6(a)-3 and (a)-4, an evenly distributed compression was observed across the four chambers in the outer layer of the fingertip sensor when compressed at  $\theta_z = 90^\circ$ . At  $4 \text{ mm}$  of indentation, the fingertip force  $F_c$  peaks at  $4.86 \text{ N}$  and the centre pressure  $P_{c(C)}$  reaches  $8.96 \text{ kPa}$ . Meanwhile, the pressures in the chambers of the outer layer of the fingertip sensor, specifically  $P_{c(UR)}$ ,  $P_{c(UL)}$ ,  $P_{c(DR)}$ , and  $P_{c(DL)}$ , reaching at approximately  $7.26 \text{ kPa}$ . In contrast, when the fingertip sensor is compressed at  $\theta_z = 80^\circ$ , as demonstrated in Fig. 6(b)-3 and (b)-4, the compression starts leaning towards the left side of the fingertip, resulting in a more intensive compression on the left-side chambers. At maximum indentation, the force on the fingertip sensor measures  $5.21 \text{ N}$ . It is noteworthy that the pressures increase in a non-linear trend with increased indentation. The left-side pressures,  $P_{c(UL)}$  and  $P_{c(DL)}$ , reach a higher level of around  $9.48 \text{ kPa}$ , similar to  $P_{c(C)}$ . In comparison, the chambers on the right side register lower pressures. The maximum pressure disparity between the left-side ( $P_{c(UL)}$  and  $P_{c(DL)}$ ) and right-side chambers ( $P_{c(UR)}$  and  $P_{c(DR)}$ ) is  $3.93 \text{ kPa}$ , observed at the maximum indentation. In Fig. 6(c) and (d), the pitch angle  $\theta_z$  is reduced to  $70^\circ$  and  $60^\circ$  respectively, leading to further inclination of compression towards the left side of the fingertip sensor. With the pitch angle set at  $70^\circ$ , the maximum force exerted on the fingertip sensor amounts to  $5.92 \text{ N}$ . In terms of pressures,  $P_{c(UL)}$  and  $P_{c(DL)}$  hit  $11.92 \text{ kPa}$ , while

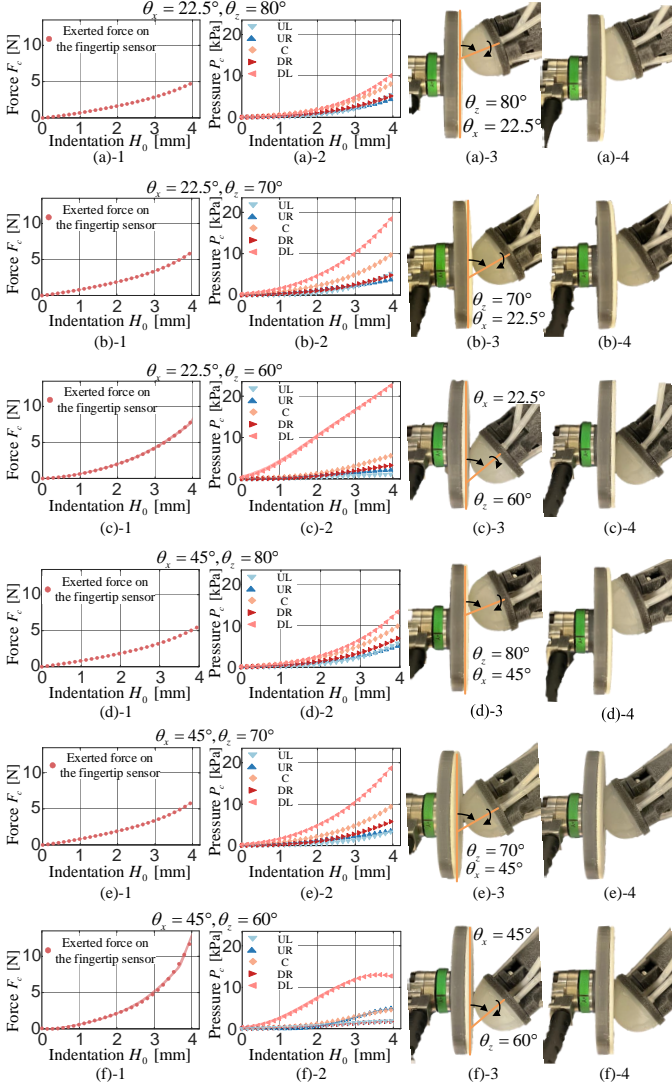


**Fig. 7.** The relationship between the force  $F_c$  and indentation  $H_0$ , the pressures  $P_c$  against the indentation  $H_0$ , the enlarged view of the fingertip sensor are compared amongst changes in rotate angle  $\theta_x$  and pitch angle  $\theta_z$ .

$P_{c(UR)}$  and  $P_{c(DR)}$  register 4.21 kPa, this at an  $H_0$  value of 4 mm. The central pressure,  $P_{c(C)}$ , reaches 9.61 kPa, while the deviation of pressure among the chambers in the outer layer expands to 7.71 kPa. In Fig. 6(d), with the pitch angle  $\theta_z$  further decreased to 60°, the maximum force on the fingertip sensor ascends to 7.27 N. The pressures,  $P_{c(UL)}$  and  $P_{c(DL)}$ , in the chambers on the left side rise to 12.65 kPa. On the other hand,  $P_{c(UR)}$  and  $P_{c(DR)}$  are considerably lower, registering at 2.66 kPa. In this scenario, the pressure deviation escalates to 10.14 kPa.

In reference to the test results shown in Fig. 6, as the pitch angle diminishes from 90° to 60°, there is a gradual increase in the force applied, scaling from 4.86 N at 90° up to 7.27 N. The pressures within the chambers of the fingertip sensor respond in diverse ways. With a decreasing pitch angle, the pressures  $P_{c(UL)}$  and  $P_{c(DL)}$  on the left side progressively rise from 7.26 kPa to 12.65 kPa. Conversely, the pressures  $P_{c(UR)}$  and

$P_{c(DR)}$  reduce from 7.26 kPa to a mere 2.66 kPa. In addition, the deviation in pressures, as compared between the left and right sides, consistently augments from 0 kPa to 10.14 kPa.

Fig. 7 shows the performance of the fingertip sensor under varying rotational ( $\theta_x$ ) and pitch ( $\theta_z$ ) angles. The results indicate an increase in force and pressure inside the sensor chambers as the pitch angle decreases from 90° to 60°, with changes in the rotational angle affecting the distribution of this pressure. Specifically, the force applied increases from 4.97 N to 14.54 N with adjustments in  $\theta_x$  and  $\theta_z$ , showcasing a complex relationship between the sensor's orientation and the mechanical forces exerted upon it. The compressed side of chambers, particularly  $P_{c(DL)}$ , consistently exhibit higher pressures, illustrating the force angle in pressure deviations. Detailed examination, such as in conditions with  $\theta_z = 80^\circ$  and  $\theta_x = 22.5^\circ$ , reveals that the lower left chamber undergoes significant compression, leading to a marked increase in pressure. This pattern becomes more pronounced with a decrease in pitch angle; at  $\theta_z = 70^\circ$ , the pressure imbalance between chambers becomes more noticeable. This illustrates the sensor's reaction to changes in its orientation, with significant variances in force and pressure responses, particularly in the chambers on the outer layer, reflecting the alteration in compression direction and intensity. Additionally, when assessing the sensor at a rotation angle of  $\theta_x = 45^\circ$ , the disparity in force and pressure across different chambers expands notably, especially as the pitch angle is reduced to 60°. This situation highlights the critical influence of increased rotational and pitch stimuli on the sensor's feedback mechanism. The force response under these angles provides indicates its capability to translate complex angular changes into distinct tactile feedback.

The results show that an increase in rotation angle  $\theta_x$  leads to an increase in both  $F_c$  and pressure deviations. Differently from the decrease in pitch angle  $\theta_z$ , a rise in  $\theta_x$  inclines the indentation direction toward a single chamber, resulting in a rapid increase in pressure compared to other chambers. In varying scenarios with different  $\theta_z$ , a larger  $\theta_x$  shifts the direction more towards the DL chamber. Specifically, at  $\theta_x = 45^\circ$  and  $\theta_z = 60^\circ$ , the compression approaches its limit, where additional compression leads to exponential increases in force without corresponding significant deformation and pressure

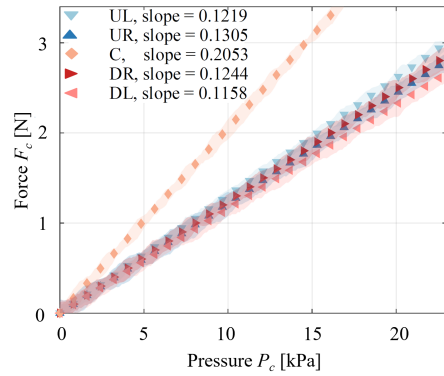


**Fig. 8.** Linear relationships between the output force at the feedback actuator and the internal liquid pressure for each linear actuator.

increase, as the sensor nears contact with the rigid support and can no longer compress the cavities in the fingertip sensor effectively. During the indentation of the fingertip sensor, the internal liquid pressure within the five cavities rises, resulting in the water medium transferring this pressure increase to the corresponding linear actuators in the feedback actuator, thus pressurising them. The resultant blocked force from each actuator, due to the pressure increase, is measured by force sensors. The linear relationships between these forces and the pressure are shown in Fig. 8, which presents summarised data from different compression cases with varying  $\theta_x$  and  $\theta_z$ . Forces from directional actuators are represented in different colours: UL (light blue), UR (dark blue), DR (dark red), and DL (light red). These relationships align with each other, displaying similar linear trends. Every directional actuator was pressurised with a maximum pressure of 23.5 kPa from the fingertip sensor. The UL chamber's pressure produces the highest value for the maximum transmitted force (2.98 N), as opposed to the DR (2.91 N), UR (2.88 N), and DL (2.74 N) chambers. The slopes of the linear relationships for the directional actuators are as follows: 0.1219 N/kPa for UL, 0.1305 N/kPa for UR, 0.1244 N/kPa for DR, and 0.1158 N/kPa for DL.

The intensify actuator, connected to the central (C) chamber in the fingertip sensor, is indicated in yellow. It has an outer diameter of 25 mm, compared to the 10 mm outer diameter of the directional actuators. The larger diameter of the intensify actuator yields a higher force output at the same pressure level. Consequently, the slope of the linear relationship for the intensify actuator is 0.2053 kPa, and it reaches a force of 3.43 N at the maximum pressure of 16.95 kPa exerted by the fingertip sensor.

### B. Experiment 2: Human interaction tests

**Protocol:** This section aims to examine participants' responses to tactile stimuli produced by the five-cavity haptic feedback system through three experimental sessions. In the first session, participants were asked to identify the source of a single tactile stimulus when a single directional chamber of the fingertip sensor was randomly compressed. In the second session, two adjacent directional chambers were simultaneously compressed, and participants had to identify the activated actuators. The final session involved varying the rotate angle  $\theta_x$  and pitch angle  $\theta_z$  of the compressed fingertip sensor, with the feedback actuator generating corresponding patterns. Participants were tasked with identifying the tactile stimulus's location based on  $\theta_x$  and  $\theta_z$ . The rotate angle  $\theta_x$  was varied from 0° to 45° in increments of 22.5°, while the pitch angle  $\theta_z$  ranged from 60° to 90°, in increments of 10°. The fingertip sensor's axisymmetry necessitated the extrapolation of the rotate angle  $\theta_x$  beyond 0° to 45°. These experiments were designed to validate the haptic feedback system's effectiveness. In total, there were six male and four female healthy participants, aged between 23 to 34 years old. The study received approval from the UCL Research Ethics Committee (application number 12453/001).

In these experiments, all participants engaged in trials involving 50 stimuli. In the first two sessions, the activated

directional actuators applied a constant force of 0.5 N, maintained for 1 s. Participants were then asked to identify the stimulus's location and specify the actuators responsible for the tactile stimuli. Their responses were recorded. In the third session, not only were participants required to identify the location and the activated actuators, but they also had to determine the pitch and rotate angles based on the force levels and patterns produced by the feedback actuator. Prior to each session, participants underwent a training session to familiarise themselves with the haptic feedback system.

The training sessions aim to enhance users' familiarity with tactile stimuli delivered by actuators from different directions and with various force patterns. Each session gradually introduces increasingly complex force patterns, starting with a single actuator touch and progressing to multiple actuators providing extensive touch. The training sessions were designed to last five minutes, during which tactile stimuli were randomly given, and users were given correct identifications. This approach helps build accurate recognition of tactile sensations.

**Test setup:** In these experiments, ten participants sat comfortably with their forearms relaxed on a table. To minimise potential external distractions, participants' visual and auditory senses were masked, allowing them to focus on tactile perception. The feedback actuator was housed in a rigid case that permitted placement of the participant's forearm and adjustment of the linear actuator's indentation direction. As depicted in Fig. 9(a), the feedback actuator was situated on the inner side of the participant's forearm, 15 cm from their wrist. Linear actuators corresponding to the fingertip sensor's upper chambers were directed towards the participant's wrist. The fingertip sensor was compressed with controlled deformation in both depth and angles ( $\theta_x$  and  $\theta_z$ ) using the workbench setup shown in Fig. 5. The angle adjustment mechanisms allowed static control of the compression angles, while the linear rail controlled the depth of compression for each trial. Fig. 6 and 7 illustrate the resulting compression angles and deformations. This setup ensured consistent and accurate control

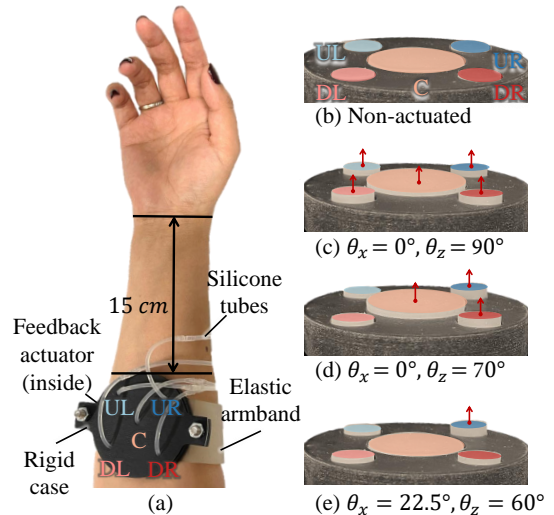


**Fig. 9.** (a) Configuration of the feedback actuator worn by one participant. (b)-(e) Actuated feedback actuator in different angle indentations at the fingertips sensor.

of the fingertip sensor's deformation during the experiment.

The force exerted on the participants by the feedback actuator in the first two sessions was precisely controlled and recorded by monitoring the liquid pressure, according to the linear relationship presented in Fig. 8. In the third session, a linear rail controlled the indentation to the fingertip sensor. Fig. 8(b) shows the resting condition of the feedback actuator. Corresponding patterns produced by the feedback actuator at different angles are displayed in Fig. 8(c), (d), and (e), which correspond to  $\theta_x = 0^\circ, \theta_z = 90^\circ$ ,  $\theta_x = 0^\circ, \theta_z = 70^\circ$ , and  $\theta_x = 22.5^\circ, \theta_z = 60^\circ$ , respectively.

**Test Results:** Fig. 10 presents confusion matrices representing the results of a single-point location test. The vertical axis denotes actual stimuli presented to the participants, while the horizontal axis reflects participants' responses. The summary on the figure's right-hand side reflects the accuracies of participant responses to each stimulus type. Correct answers, which align with actual stimuli, are highlighted in blue cells. Alternatively, red cells represent erroneous responses, indicating participant confusion. In the first session, ten participants underwent testing with a total of 522 stimuli. Fig. 10(a) reveals a proficiency of 93.93% in accurately identifying stimulated fingertip locations corresponding to feedback actuators at four distinct locations. The precision for UL, UR, DR, and DL locations was fairly uniform, at 90.5%, 96.3%, 95.7%, and 93.2%, respectively. The tactile stimuli could be correctly discerned at all four locations in most cases. Participant errors appear to be evenly and randomly distributed across the figure, showing no discernible pattern.

During the second session, a total of 500 stimuli were administered to ten participants. The overall accuracy in identifying two activated actuators in the feedback from the stimulated fingertip was 89.35%, as shown in Fig. 10(b). The case of UL & UR, UL & DL, UR & DR, and DR & DL demonstrated the accuracy levels of 89.9%, 92.9%, 87.9%, and 86.7%, respectively. For UL & UR stimuli, 8 of 14 errors were

mistakenly identified as UL & DL. The remaining errors were dispersed across the figure, with only one or two instances per error. Despite these errors, most two-point stimuli could be correctly identified by the participants.

In the final session, participants were tasked with distinguishing the rotate angle  $\theta_x$  and pitch angle  $\theta_z$  of the compressed fingertip sensor, based on the inflation patterns produced by the feedback actuator. ten participants undertook the test, which consisted of 500 stimuli in total. Fig. 10(c) shows the results. On average, the accuracy of the participants in distinguishing the angles was 45.29%. The instances of  $(22.5^\circ, 80^\circ)$  yielded highest accuracies of 71.4%, whereas the  $(22.5^\circ, 70^\circ)$  scenario produced the lowest accuracy at 25.4%. The layout of the horizontal and vertical axes is in descending order of  $\theta_z$ , and within each  $\theta_z$ ,  $\theta_x$  varies in  $0^\circ, 22.5^\circ$ , and  $45^\circ$ . The confusion errors in this session were generally located within a deviation of three cases on either side of the correct answers.

### C. Experiment 3: Usability test

**Protocol:** This section aims to validate the usability of the proposed multi-cavity fluidic haptic feedback system for upper-limb prostheses. As shown in Fig. 11(a), the haptic feedback system has been integrated into body-powered prosthesis. In Fig. 11(b), during the tests, participants were instructed to use the prosthetic hand to grasp and lift objects, then hold the item for five seconds. Meanwhile, participants perceived tactile stimuli. After the trial, all participants answered two questions regarding:

- The usefulness of the haptic feedback system: “Not useful (1)”, “Slightly useful (2)”, “Useful (3)”, “Fairly useful (4)”, “Very useful (5)”.
- The difficulty to identify the direction: “Not easy (1)”, “Slightly easy (2)”, “Easy (3)”, “Fairly easy (4)”, “Very easy (5)”.

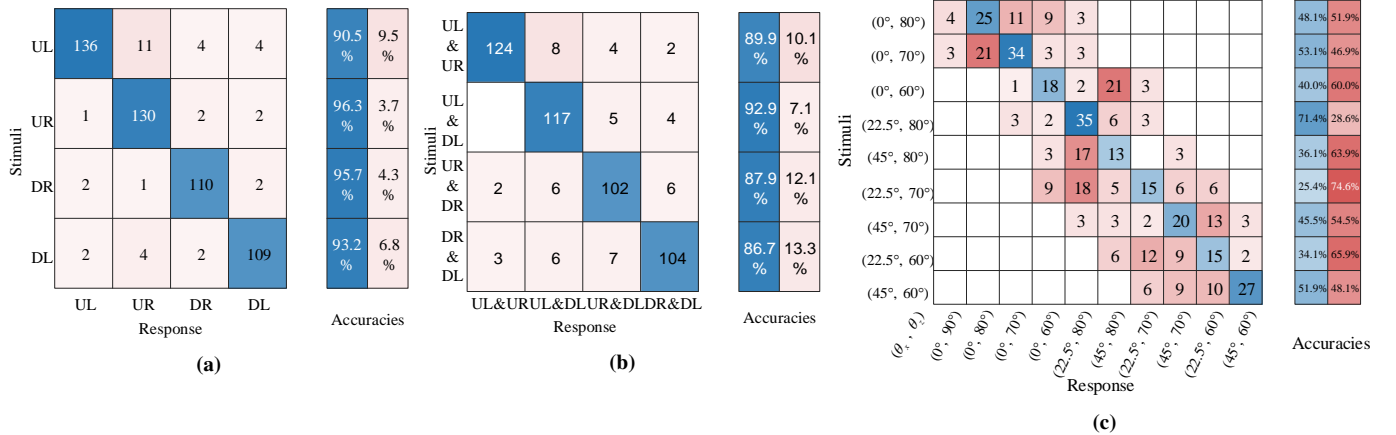


**Fig. 10.** Confusion matrices for tests with summarised results from participants. (a) One-point location test: four points were required to identify from the feedback actuator, which are UL, UR, DR, and DL, respectively. (b) Two-point location test: Four cases were required to identify from the feedback actuator: UL & UR, UL & DL, UR & DR, and DR & DL, respectively. (c) Angle identification test: Participants are required to identify and compression angle of in the fingertip sensor. The rotate angle  $\theta_x$  varies in a range of  $0^\circ$  to  $45^\circ$  degrees with a  $22.5^\circ$  interval, and the pitch angle  $\theta_z$  varies in a range from  $60^\circ$  to  $90^\circ$  with a  $10^\circ$  interval.

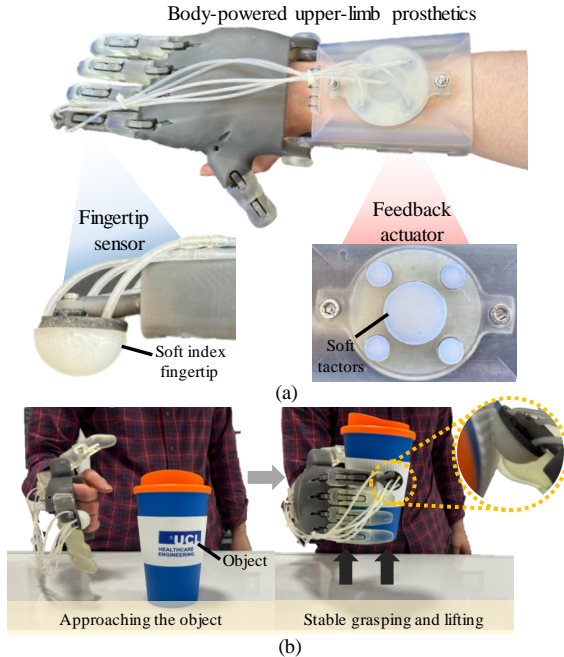


**Fig. 11.** (a) Configuration of the multi-cavity fluidic haptic feedback system integrated into body-powered upper-limb prosthesis. The sensor is integrated into the tip of the index finger, and the feedback actuator is mounted on the arm guard. (b) Demonstration of the experimental setup for the usability test: A healthy participant wears the prosthetic integrated with the haptic feedback system, then grasps and lifts an object, sensing the tactile stimuli.

In total, there were six male and four female healthy participants, aged between 23 to 34 years old.

*Test setup:* All healthy participants were wearing the e-NABLE body-powered prosthetic hand, fitted over their healthy hand and forearm. The prosthetic hand was 3D printed using a Form 3+ printer from Formlabs Inc. The fingertip sensor was integrated into the tip of the index finger. During the operation, as the prosthetic hand grasped an object, the fingertip sensor deformed and pressurised the feedback actuator. Consequently, the haptic actuators inflated to create various force patterns, compressing the skin tissue of the user. The feedback actuator was positioned approximately 15 cm from their wrist.

*Test Results:* During the test, all participants were able to feel the mechano-tactile stimuli from the haptic feedback system during the grasping. Fig. 12 demonstrates the results of the usability test. Fig. 12(a) indicates the difficulty in identifying the directions, where the average score is 2.5, positioned between “Easy” and “Slightly Easy”. Two out of ten participants given the highest score, “Fairly Easy”, while two participants assigned the score of “Not Easy”, amounting to a score of 1. The remaining participants rated the difficulty as “Slightly Easy” and “Easy”. Fig. 12(b) presents the feedback on the usefulness of the system from participants, with an average score of 2.4, bordering between “Useful” and “Slightly Useful”. One participant awarded the highest score of “Fairly Useful”, and two participants rated it as “Not Useful”. The remaining participants provided scores of “Slightly Useful” and “Useful”.

## V. DISCUSSION

The system is purely hydraulically driven, utilising silicone moulding as its manufacturing method. This approach simplifies the production process by excluding electronic components, reducing the manufacturing cost to under \$5, which includes the cost of silicone-based soft structures and pipes. With the adoption of modern manufacturing techniques, such as injection moulding, there is potential for further cost reduction. The system’s weight is 25.4 g when fully filled with water, and it can operate at an internal pressure of 22.85 kPa without sustaining damage. The average weight of an AA battery is 25.4 g [46]. The proposed haptic feedback system operates without a battery, making it lighter than an AA battery, for comparison. Moreover, our multi-cavity fluidic system, which solely utilises skin-friendly silicone, significantly reduces costs compared to traditional electronic haptic systems. Our fabrication process is notably simpler, eliminating the need for complex electronic manufacturing steps, such as soldering. Compared to existing devices, this system is more affordable and features a simpler structure, comprising only a fingertip sensor and a feedback actuator.

In Section IV, the multi-chamber haptic feedback system is validated and characterised its capability to provide feedback force in different directions. By compressing the multi-cavity fingertip sensor at various pitch angles  $\theta_z$  and rotation angles  $\theta_x$ , the notable pressure deviation appears allowing the feedback actuator to generate different haptic patterns. When the fingertip sensor is positioned at  $\theta_z = 90^\circ$ , the sensor experiences compression vertically in the normal direction, leading to a non-linear increase in the force exerted on the sensor and the pressures within the chambers. Further compression of the fingertip sensor results in heightened pressure, which in turn stiffens the sensor. This leads to a more significant force and pressure increase during subsequent indentation steps.

As the pitch angle  $\theta_z$  decreases from  $90^\circ$  to  $60^\circ$ , the indentation direction on the fingertip sensor starts to incline. This results in chambers facing the contact plate experiencing more significant compression compared to the other chambers. When the rotation angle  $\theta_x = 0^\circ$  and the pitch angle  $\theta_z$  decreases, the two adjacent chambers facing the contact plate are compressed equally, while the remaining chambers experience less compression compared to when compressed in the normal direction. As a result, the pressures within the chambers facing the contact plate increase more substantially, while the pressures within the remaining chambers of the fingertip sensor exhibit relatively smaller increases. This variation in pressure serves as an indicator of the compression angle.

As the rotation angle  $\theta_x$  increases, the compression starts to incline towards a single chamber. This results in the chamber facing the contact plate experiencing a greater degree of compression compared to the other chambers. Consequently, the pressure within the inclined chamber experiences a sharp increase, leading to a noticeable pressure deviation. This surge in pressure within a single chamber indicates a change in the rotation angle. However, when  $\theta_z = 60^\circ$  and  $\theta_x = 45^\circ$ , the fingertip sensor reaches its compression limit, as the indentation does not lead to sufficient deformation, and the

pressure fails to increase proportionally. Although the pressure deviation continues to reflect the rotation of the fingertip sensor, the amplitude of the pressure level no longer accurately represents the depth of indentation.

With the directional chamber at a indentation of 1.5, mm, a noticeable increase in pressure within the central chamber begins. This pressure then rises exponentially as the fingertip continues to compress, eventually coming into contact with the inner layer of the fingertip sensor. Given an indentation depth of the fingertip sensor at 4, mm, the directional chamber becomes fully compressed. However, the central chamber can still endure further compression. After the inner cavity deforms, pressurising the central chamber in the feedback actuator, it triggers the actuator to signal an intense touch. As a result, a pressure disparity is observed between the central and directional chambers. The central chamber often exhibits lower pressure relative to the peak pressure recorded in the directional chamber.

In summary, the fingertip sensor efficiently discerns the force direction by tracking pressure variances. A reduction in the pitch angle  $\theta_z$  correlates with a rise in the peak pressure within the directional chamber, resulting in a pressure variation as the pressure in the two adjacent chambers increases concurrently. An elevation in the rotation angle  $\theta_x$  induces a more substantial pressure difference in one chamber relative to the others. Hence, the force direction can be inferred by observing these pressure discrepancies within the fingertip sensor.

Within this haptic feedback system, feedback actuators generate corresponding patterns based on the compression of the fingertip sensor. Pressure deviations in the fingertip sensor's outer layer are mirrored in the directional chambers of the feedback actuator. Here, pressure acts as the signal, and incompressible water serves as the signal medium, transferring the pressure from the fingertip sensor to the feedback actuator. This pressure deviation within the fingertip sensor results in a force variation in the feedback actuator. For instance, when the fingertip sensor is compressed at angles  $\theta_x = 22.5^\circ$  and  $\theta_z = 60^\circ$ , a pressure deviation of 14.95, kPa is observed in the directional chambers at a 3, mm indentation. As depicted in Fig. 8, this pressure difference of 14.95, kPa induces a 1.79, N force discrepancy, with the free inflation difference shown in Fig. 9(e). Thus, users can recognise the respective patterns to determine the angle of the fingertip sensor.

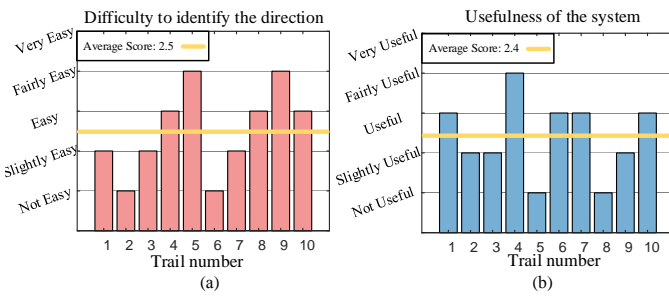


**Fig. 12.** Results for Experiment 3: Usability test results of ten participants. (a) Assessment of the device operation with regards to difficulty. (b) Usefulness evaluation of the grasping. Yellow lines denote the average values.

In the first session of the human interaction test, participants were tasked with identifying the location of the activated linear actuator, representative of the compressed directional chamber. Following a training session, all ten participants successfully determined the location corresponding to the compressed portion of the fingertip. The confusion errors associated with each stimulus were evenly dispersed across the confusion matrix. Consequently, these errors can be regarded as sporadic or random, rather than systematic inaccuracies. This suggests the haptic feedback system is generally successful in conveying information concerning the direction of the applied force. Moreover, users can accurately decipher the corresponding patterns after undergoing suitable training. The system is able to produce forces up to 2.9 N using directional chambers. For non-directional forces, the enhance chamber can generate an additional 3.4 N on the target skin tissue, acting as a force level indicator for user.

In the second session of the human interaction test, following the training phase, participants were asked to identify the two activated adjacent chambers. This session revealed similarities with the initial session, as participants displayed the ability to discern the side of the compression applied to the fingertip sensor, achieving a satisfactory success rate. Confusion errors were found to be randomly distributed within the confusion matrix, manifesting as sporadic errors, except in cases where the stimulating chambers were Upper Left (UL) & Upper Right (UR), but were misidentified as Upper Left (UL) & Lower Left (DL). In these instances, participants successfully recognised the common chamber (UL), but encountered difficulty in distinguishing between the Upper Left (UL) and Upper Right (UR) chambers. As a result, the success rate for two-point discrimination was found to be acceptable.

In the final session of the human interaction test, participants were tasked with identifying both the direction of compression and the compression angles  $\theta_x$  and  $\theta_z$ . Throughout the test, the fingertip was subjected to a 3, mm indentation. As varying compression angles were applied, the fingertip sensor registered differing pressure deviations, as depicted in Fig. 6 and Fig. 7. These pressure deviation led to the emergence of unique patterns within the feedback actuator.

As the pitch angle  $\theta_z$  decreased from  $90^\circ$  to  $60^\circ$ , while the rotation angle  $\theta_x$  remained constant at  $90^\circ$ , an increase in pressure was observed in two adjacent directional actuators. This change, in turn, led to an increase in force emanating from the corresponding linear actuators as depicted in Fig. 9(d). The force difference in the feedback actuator escalated to 1.18, N at  $\theta_z = 60^\circ$  when compared between the side inclining towards the contact plate and the side opposite the contact plate. Simultaneously, as  $\theta_z$  dropped from  $90^\circ$  to  $60^\circ$ , the pressure within the intensification chamber declined, resulting in the force output decreasing from 1.974, N to 1.21, N.

Generally, as  $\theta_z$  decreased, the force patterns generated by the feedback actuator transitioned from uniformly activated actuators to the activation of a single-sided actuator, while the force produced by the intensification actuator decreased. Considering that participants were able to identify two-point stimuli in the second session, they were also capable of determining against which two points the fingertip sensor was

compressed. Nevertheless, during the angle determination test in the third session, the success rate for detecting  $\theta_z$  when  $\theta_x = 0^\circ$  was 55.63%, a figure that is regarded as acceptable.

Analogous to the variations in  $\theta_z$ , an increase in the rotation angle  $\theta_x$  results in the compression direction inclining towards a single directional chamber, consequently leading to a rise in the corresponding cavity pressure. As a result, a single linear actuator within the feedback actuator is activated, signifying the compressed direction of the fingertip sensor. The pressure deviation of the fingertip sensor within a single chamber escalates to 18.97, kPa, causing the force deviation to increase to 2.35, N.

In comparison to cases where the fingertip sensor experiences compression in the normal direction (with all actuators activated) or those with only a change in the pitch angle  $\theta_z$  (involving two adjacent actuators), an increase in the rotation angle  $\theta_x$  yields pressure deviation concentrated in a single chamber, resulting in the activation of a single linear actuator. Consequently, participants become aware of the rise in  $\theta_x$  by identifying that only one point of the actuator is stimulated. Simultaneously, as  $\theta_x$  increases, the pressure in the intensification actuator also increases, assisting participants in recognising the one-point stimulation.

According to the feedback from participants, she feedback actuator can generate forces up to approximately 2.9 N for directional feedback and 3.4 N for non-directional feedback. These forces correspond to the sensation of having a small object pressing against the skin. For example, 2.9 N feels similar to pressing the tip of an index finger firmly against the skin or the weight of a smartphone resting on the skin. Similarly, 3.4N can be compared to the pressure felt when a finger presses firmly against the skin or the weight of a tablet on the skin.

Overall, in the angle identification test involving an increase in  $\theta_x$  and a decrease in  $\theta_z$ , the average accuracy stands at 47.92%, which is lower than the accuracy achieved when only  $\theta_z$  changes. This discrepancy may be attributed to the increased number of cases and instances where small differences in  $\theta_x$  and  $\theta_z$  values fail to generate sufficient force differences for participants to discern.

Experiment 3 aimed to validate the usability of the multi-cavity fluidic haptic feedback system designed for upper-limb prosthetics. In this experiment, participants, fitted with the e-NABLE body-powered prosthetic hand, performed tasks that involved grasping and lifting objects while experiencing tactile stimuli generated by the haptic feedback system. The results of this experiment demonstrate that all participants could perceive the tactile stimuli during grasping, indicating the system's potential to enhance the perception of touch in prosthetic users. The average scores for the difficulty in identifying the direction and the usefulness of the system were 2.5 and 2.4, respectively, suggesting that while the system provided some level of tactile feedback, there is room for improvement in making the stimuli more distinguishable and useful.

According to the participants' feedback, they were able to clearly perceive the tactile stimuli during the object approach stage. By adjusting the prosthetic to different positions for grasping, they could identify the direction of touch. When the

lower chamber of the fingertip sensor was actuated, participants inferred that the prosthetic hand had achieved stable grasping, contributing to a more reliable grasping function for upper-limb amputees. Conversely, some participants suggested that the haptic feedback system needs to generate more intense tactile stimuli to clearly identify the touch location. As body-powered prosthetics require some force to actuate, the movement of their skin might diminish the tactile sensations they perceive. Additionally, although participants could feel the intensification actuator, it was activated during stable grasping of an object, at which point they exerted significant force. Some participants suggested that increasing the levels of force feedback could improve force accuracy, enabling them to apply a more precise force on the object. The feedback provided by the participants aligns with findings in existing research, indicating that initial usability scores suggest the system's fundamental design and operational concepts are effective [26]. For instance, a study on the usability of haptic feedback systems highlighted that participants' ability to feel and interpret tactile feedback is a significant indicator of the system's potential. Thus, while participants identified areas for improvement, their ability to perceive and respond to the tactile stimuli validates the functionality and foundational usability of the system. These insights provide a baseline for future refinements, ensuring that the system can be improved to enhance the user experience [47].

## VI. CONCLUSIONS

This paper presented an optimised fluidic haptic feedback system, featuring a five-chamber fingertip sensor and feedback actuator. This design equips the haptic feedback system with the capability to communicate both the direction and magnitude of the applied force. A comprehensive demonstration of the system's design and fabrication process has been detailed.

The fingertip sensor is composed of five cavities, with four chambers located in the outer layer to denote the direction of the force. A single chamber in the inner layer serves as an intensifier to augment the haptic sensation. The feedback actuator consists of five linear actuators, each individually connected to the five cavities within the fingertip sensor. To regulate the direction of inflation and reduce lateral inflation, the linear actuator implements a thread reinforcement method. The design of both the fingertip sensor and feedback actuator incorporates silicone into the fingertip and actuator membrane. These two components are connected through a tube filled with a hydraulic medium, transferring pressure transfer between the fingertip and the feedback actuator.

The system was evaluated and validated through three experiments. The first experiment assessed the system and established the relationship between the fingertip sensor and feedback actuator. This system is capable of detecting physical touch with exerted direction, conveyed as pressure deviations across the five cavities. Meanwhile, the pressures within the five cavities were transferred to the feedback actuator, generating corresponding forces in response to applied pressure. The force discrepancies among the five linear actuators reflect the force direction and magnitude sensed by the fingertip sensor.

The second experiment involved testing the haptic feedback system with ten healthy participants to verify its ability to detect and convey the force with direction, as well as to ensure users can perceive tactile stimuli. Three sessions were designed for this assessment. The first session demonstrated the system's capacity to sense one-point stimulation, while the second session illustrated its capability to convey two-point stimuli. In the third session, participants were tasked with identifying the force direction based on the force patterns generated by the feedback actuator. The results show that participants can generally detect changes in angle.

The outcomes from Experiment 3 suggest that the integrated haptic feedback system can potentially improve the functionality of body-powered prosthetics, offering users a better grasp and awareness of the items they are handling. In future work, the haptic feedback system will need to be validated with upper-limb amputees. We aim to enhance the adaptability of our haptic feedback system to fit to a wider range of amputation conditions by exploring various target locations beyond the forearm, particularly for those with partial amputations with skin tissue having higher tactile sensitivity. The haptic feedback system may be optimised with different force level to allow the users to apply a more precise force on the different object. Piping of the proposed system need to be enhanced to fit into prostheses in the future.

#### ACKNOWLEDGMENT

This research has been supported by the Grand Challenges Small Grant received from UCL Grand Challenges, the Royal Academy of Engineering - Industry-Academia Partnership Programme Colombia/UK (IAPP18-19\264), the Engineering and Physical Sciences Research Council (grant number: EP/V01062X/1) and UCL-IIT Delhi Seed Funding 2020-21 received from UCL Global Engagement.

#### REFERENCES

- [1] W. H. Organization and Others, "Guidelines for training personnel in developing countries for prosthetics and orthotics services," 2005.
- [2] W. H. Organization, *Global status report on road safety 2015*. World Health Organization, 2015.
- [3] B. S. of Rehabilitation Medicine, *Amputee and Prosthetic Rehabilitation: Standards and Guidelines*. BSRM, 2003.
- [4] I. Imbianto, C. Peccia, M. Controzzi, A. G. Cutti, A. Davalli, R. Sacchetti, and C. Cipriani, "Treatment of the partial hand amputation: an engineering perspective," *IEEE Reviews in Biomedical Engineering*, vol. 9, pp. 32–48, 2016.
- [5] E. A. Biddiss, *A framework for user-based design in upper extremity prostheses: Consumer profiling and evaluation of electroactive polymers as prosthetic actuators and sensors*, 2007.
- [6] M. N. Nemah, C. Y. Low, O. H. Aldulaymi, P. Ong, A. A. Qasim *et al.*, "A review of non-invasive haptic feedback stimulation techniques for upper extremity prostheses," *International Journal of Integrated Engineering*, vol. 11, no. 1, 2019.
- [7] E. D. Engeberg, S. Dilibal, M. Vatani, J.-W. Choi, and J. Lavery, "Anthropomorphic finger antagonistically actuated by sma plates," *Bioinspiration & Biomimetics*, vol. 10, no. 5, 2015.
- [8] L. Resnik, M. Borgia, J. Cancio, J. Heckman, J. Highsmith, C. Levy, S. Phillips, and J. Webster, "Dexterity, activity performance, disability, quality of life, and independence in upper limb veteran prosthesis users: a normative study," *Disability and Rehabilitation*, vol. 44, no. 11, pp. 2470–2481, 2022.
- [9] L. Resnik, M. Borgia, and M. Clark, "Function and quality of life of unilateral major upper limb amputees: effect of prosthesis use and type," *Archives of Physical Medicine and Rehabilitation*, vol. 101, no. 8, pp. 1396–1406, 2020.
- [10] J. S. Schofield, K. R. Evans, J. P. Carey, and J. S. Hebert, "Applications of sensory feedback in motorized upper extremity prostheses: a review," *Expert Review of Medical Devices*, vol. 11, no. 5, pp. 499–511, 2014.
- [11] P. Svensson, U. Wijk, A. Björkman, and C. Antfolk, "A review of invasive and non-invasive sensory feedback in upper limb prostheses," *Expert Review of Medical Devices*, vol. 14, no. 6, pp. 439–447, 2017.
- [12] J. W. Sensinger and S. Dosen, "A review of sensory feedback in upper-limb prostheses from the perspective of human motor control," *Frontiers in Neuroscience*, vol. 14, p. 345, 2020.
- [13] K. Kim and J. E. Colgate, "Haptic feedback enhances grip force control of semg-controlled prosthetic hands in targeted reinnervation amputees," *IEEE Transactions on Neural Systems and Rehabilitation Engineering*, vol. 20, no. 6, pp. 798–805, 2012.
- [14] N. Colella, M. Bianchi, G. Grioli, A. Bicchi, and M. G. Catalano, "A novel skin-stretch haptic device for intuitive control of robotic prostheses and avatars," *IEEE Robotics and Automation Letters*, vol. 4, no. 2, pp. 1572–1579, 2019.
- [15] J. Wheeler, K. Bark, J. Savall, and M. Cutkosky, "Investigation of rotational skin stretch for proprioceptive feedback with application to myoelectric systems," *IEEE Transactions on Neural Systems and Rehabilitation Engineering*, vol. 18, no. 1, pp. 58–66, 2010.
- [16] C. Antfolk, C. Cipriani, M. C. Carrozza, C. Balkenius, A. Björkman, G. Lundborg, B. Rosén, and F. Sebelius, "Transfer of tactile input from an artificial hand to the forearm: experiments in amputees and able-bodied volunteers," *Disability and Rehabilitation: Assistive Technology*, vol. 8, no. 3, pp. 249–254, 2013.
- [17] R. Zhou, Z. Schwemler, A. Bawej, H. Sareen, C. L. Hunt, and D. Leitinger, "Tactorbots: a haptic design toolkit for out-of-lab exploration of emotional robotic touch," in *Proceedings of the CHI Conference on Human Factors in Computing Systems*, 2023, pp. 1–19.
- [18] C. P. Premaratna, D. S. Chathuranga, and T. D. Lalitharatne, "Fabrication of a soft tactile display based on pneumatic balloon actuators and voice coils: Evaluation of force and vibration sensations," in *IEEE/SICE International Symposium on System Integration*, 2017, pp. 763–768.
- [19] C. P. Premaratna, I. Ruhanage, D. S. Chathuranga, and T. D. Lalitharatne, "Haptic feedback system for an artificial prosthetic hand for object grasping and slip detection: A preliminary study," in *IEEE International Conference on Robotics and Biomimetics*, 2018, pp. 2304–2309.
- [20] M. Zhu, S. Biswas, S. I. Dinulescu, N. Kastor, E. W. Hawkes, and Y. Visell, "Soft, wearable robotics and haptics: Technologies, trends, and emerging applications," *Proceedings of the IEEE*, vol. 110, no. 2, pp. 246–272, 2022.
- [21] F. Barontini, M. G. Catalano, G. Grioli, M. Bianchi, and A. Bicchi, "Wearable integrated soft haptics in a prosthetic socket," *IEEE Robotics and Automation Letters*, vol. 6, no. 2, pp. 1785–1792, 2021.
- [22] J. J. Huaroto, E. Suarez, H. I. Krebs, P. D. Marasco, and E. A. Vela, "A soft pneumatic actuator as a haptic wearable device for upper limb amputees: Toward a soft robotic liner," *IEEE Robotics and Automation Letters*, vol. 4, no. 1, pp. 17–24, 2019.
- [23] M. Zhu, A. H. Memar, A. Gupta, M. Samad, P. Agarwal, Y. Visell, S. J. Keller, and N. Colonnese, "Pneusleeve: In-fabric multimodal actuation and sensing in a soft, compact, and expressive haptic sleeve," in *Proceedings of the CHI Conference on Human Factors in Computing Systems*, 2020, pp. 1–12.
- [24] A. Shtarbanov, M. Zhu, N. Colonnese, and A. Hajiagha Memar, "Sleeveio: modular and reconfigurable platform for multimodal wearable haptic feedback interactions," in *Proceedings of the ACM Symposium on User Interface Software and Technology*, 2023, pp. 1–15.
- [25] D. S. Childress, "Closed-loop control in prosthetic systems: historical perspective," *Annals of Biomedical Engineering*, vol. 8, pp. 293–303, 1980.
- [26] C. Antfolk, A. Björkman, S.-O. Frank, F. Sebelius, G. Lundborg, and B. Rosen, "Sensory feedback from a prosthetic hand based on air-mediated pressure from the hand to the forearm skin," *Journal of Rehabilitation Medicine*, vol. 44, no. 8, p. 702, 2012.
- [27] G. Shi, A. Palombi, Z. Lim, A. Astolfi, A. Burani, S. Campagnini, F. G. Loizzo, M. L. Preti, A. M. Vargas, E. Peperoni *et al.*, "Fluidic haptic interface for mechano-tactile feedback," *IEEE Transactions on Haptics*, vol. 13, no. 1, pp. 204–210, 2020.
- [28] G. Shi, A. Shariati, I. Eames, and H. Wurdemann, "Modelling the compression of a soft ellipsoid fingertip," *Soft Matter*, vol. 18, no. 47, pp. 9076–9085, 2022.
- [29] L. Vargas, H. Huang, Y. Zhu, and X. Hu, "Object recognition via evoked sensory feedback during control of a prosthetic hand," *IEEE Robotics and Automation Letters*, vol. 7, no. 1, pp. 207–214, 2021.

- [30] P. G. S. Alva, S. Muceli, S. F. Atashzar, L. William, and D. Farina, “Wearable multichannel haptic device for encoding proprioception in the upper limb,” *Journal of Neural Engineering*, vol. 17, no. 5, 2020.
- [31] H. Cha, S. An, S. Choi, S. Yang, S. Park, and S. Park, “Study on intention recognition and sensory feedback: Control of robotic prosthetic hand through emg classification and proprioceptive feedback using rule-based haptic device,” *IEEE Transactions on Haptics*, vol. 15, no. 3, pp. 560–571, 2022.
- [32] M. A. Abd, J. Ingicco, D. T. Hutchinson, E. Tognoli, and E. D. Engeberg, “Multichannel haptic feedback unlocks prosthetic hand dexterity,” *Scientific Reports*, vol. 12, no. 1, p. 2323, 2022.
- [33] Y. H. Jung, J.-Y. Yoo, A. Vázquez-Guardado, J.-H. Kim, J.-T. Kim, H. Luan, M. Park, J. Lim, H.-S. Shin, C.-J. Su *et al.*, “A wireless haptic interface for programmable patterns of touch across large areas of the skin,” *Nature Electronics*, vol. 5, no. 6, pp. 374–385, 2022.
- [34] K. Suzumori, S. Endo, T. Kanda, N. Kato, and H. Suzuki, “A bending pneumatic rubber actuator realizing soft-bodied manta swimming robot,” in *Proceedings 2007 IEEE International Conference on Robotics and Automation*, 2007, pp. 4975–4980.
- [35] A. Shiva, A. Stilli, Y. Noh, A. Faragasso, I. D. Falco, G. Gerboni, M. Cianchetti, A. Menciassi, K. Althoefer, and H. A. Wurdemann, “Tendon-based stiffening for a pneumatically actuated soft manipulator,” *IEEE Robotics and Automation Letters*, vol. 1, no. 2, pp. 632–637, 2016.
- [36] J. Shi, J. C. Frantz, A. Shariati, A. Shiva, J. S. Dai, D. Martins, and H. A. Wurdemann, “Screw theory-based stiffness analysis for a fluidic-driven soft robotic manipulator,” in *IEEE International Conference on Robotics and Automation*, 2021, pp. 11938–11944.
- [37] J. Shi, S.-A. Abad, A. Menciassi, K. Althoefer, and H. A. Wurdemann, “Miniatuerised soft manipulators with reinforced actuation chambers on the sub-centimetre scale,” in *2024 IEEE 7th International Conference on Soft Robotics (RoboSoft)*, 2024, pp. 157–164.
- [38] J. Shi, A. Shariati, S.-A. Abad, Y. Liu, J. S. Dai, and H. A. Wurdemann, “Stiffness modelling and analysis of soft fluidic-driven robots using lie theory,” *The International Journal of Robotics Research*, vol. 43, no. 3, pp. 354–384, 2024.
- [39] W. Gaozhang, Y. Li, J. Shi, Y. Wang, A. Stilli, and H. Wurdemann, “A novel stiffness-controllable joint using antagonistic actuation principles,” *Mechanism and Machine Theory*, vol. 196, p. 105614, 2024.
- [40] J. Peters, B. Anvari, J. Licher, M. Wiese, A. Raatz, and H. A. Wurdemann, “Acceptance and usability of a soft robotic, haptic feedback seat for autonomy level transitions in highly automated vehicles,” *IEEE Transactions on Haptics*, pp. 1–15, 2024.
- [41] J. Fraś, J. Czarnowski, M. Maciąś, J. Główka, M. Cianchetti, and A. Menciassi, “New stiff-flop module construction idea for improved actuation and sensing,” in *IEEE International Conference on Robotics and Automation (ICRA)*. IEEE, 2015, pp. 2901–2906.
- [42] J. Fras and K. Althoefer, “Soft fiber-reinforced pneumatic actuator design and fabrication: Towards robust, soft robotic systems,” in *Towards Autonomous Robotic Systems: 20th Annual Conference (TAROS)*. Springer, 2019, pp. 103–114.
- [43] S. J. Lederman and R. L. Klatzky, “Haptic perception: A tutorial,” *Attention, Perception, & Psychophysics*, vol. 71, no. 7, pp. 1439–1459, 2009.
- [44] B. P. Delhaye, F. Schiltz, A. Barrea, J.-L. Thonnard, and P. Lefèvre, “Measuring fingerpad deformation during active object manipulation,” *Journal of Neurophysiology*, vol. 126, no. 4, pp. 1455–1464, 2021.
- [45] N. Nakazawa, Y. Uekita, H. Inooka, and R. Ikeura, “Experimental study on human’s grasping force,” in *IEEE International Workshop on Robot and Human Communication*. IEEE, 1996, pp. 280–285.
- [46] M. F. Almeida, S. M. Xará, J. Delgado, and C. A. Costa, “Characterization of spent aa household alkaline batteries,” *Waste Management*, vol. 26, no. 5, pp. 466–476, 2006.
- [47] B. Stephens-Fripp, G. Alici, and R. Mutlu, “A review of non-invasive sensory feedback methods for transradial prosthetic hands,” *IEEE Access*, vol. 6, pp. 6878–6899, 2018.



**Ge Shi** received the B.S. degree in Electrical & Electronic Engineering from the University of Strathclyde, UK, in 2016 and the M.S. degree in Power System Engineering from the University College London, UK, in 2017. He obtained the PhD in Mechanical Engineering at University College London, UK in 2023. He is a CERC Fellow at Data61, Commonwealth Scientific and Industrial Research Organisation (CSIRO), Australia. His research interests include soft robotics, medical devices and Artificial Intelligence.



**Jialei Shi** received the B.S. degree in Naval Architecture and Ocean Engineering from the Harbin Institute of Technology, China, in 2017, and the M.S. degree in Aerospace Engineering from the Beijing Institute of Technology, China, in 2019, and PhD in Mechatronic and Robotic Engineering from the University College London, UK, in 2024. He is currently a Research Associate in the Hamlyn Centre for Robotic Surgery, Imperial College London, UK. His research interests include design, modelling and control of soft robotics and medical devices.



**Azadeh Shariati** received her BSc, MSc, and PhD in Mechanical Engineering from Khajeh Nasir Toosi University and Sharif University of Technology, Iran. In 2016, she pursued her research as a postdoctoral researcher in the field of Social and Cognitive Robotics at Sharif University. She was also an assistant professor in Robotics and Biomedical Engineering at Islamic Azad University North Tehran Branch from 2016–2019. In 2019, she joined the Intelligent Mobility Group/Lab (IM@UCL) and Soft Haptics and Robotics Lab at University College London.



**Kamyar Motaghedolhagh** received his BSc and MSc in Mechanical Engineering from the University of Guilan, and Sharif University of Technology, Iran. He is currently pursuing his PhD degree in Mechanical Engineering at University College London, London, UK. He has more than 10 years of experience in R&D projects in academic research centres. His research interests include soft robotics, medical devices, and computational fluid dynamics.



**Shervanthi Homer-Vanniasinkam** is a Consultant Vascular Surgeon with Leeds Teaching Hospitals NHS Trust; the Founding Professor of Surgery with the University of Warwick Medical School, and University Hospitals Coventry and Warwickshire; and a Professor of Engineering and Surgery with University College London. She is also a Visiting Scholar with Harvard University, the Yeoh Ghim Seng Visiting Professor of Surgery with the National University of Singapore, and the Brahm Prakash Visiting Professor with the Indian Institute of Science.



**Helge A. Wurdemann** is Professor of Robotics, Turing Fellow (2021-2023) and leads the Soft Haptics and Robotics lab in the Department of Mechanical Engineering at University College London. Prior, he received a degree (Dipl.-Ing.) in electrical engineering with a focus on mechatronics and robotics in the medical field from the Leibniz University of Hanover, and a PhD in Robotics from King's College London in 2012. Helge has authored over 100 articles, published in high-impact journals, and peer-reviewed full-length conference papers.